Supporting Information

Exploring the role of adsorption and surface state on the hydrophobicity of rare earth oxides

Ross Lundy[*,1,2], Conor Byrne[3], Justin Bogan[3], Kevin Nolan[1], Maurice N. Collins[2], Eric Dalton[2] and Ryan Enright[*,1]

[1]Thermal Management Research Group, Efficient Energy Transfer (ηET) Dept., Bell Labs Ireland, Nokia, Blanchardstown Business & Technology Park, Snugborough Rd. Dublin 15, Ireland
[2]Stokes Laboratories, University of Limerick, Co. Limerick, Ireland
[3]School of Physical Sciences, Dublin City University, Glasnevin, Dublin 9, Ireland
*** Corresponding author: ross.lundy2@gmail.com, ryan.enright@nokia.com**

Section S1 – XPS

Peak Fitting

Normal emission (90°) and off-angle (30°) emission spectra were acquired, however only off-angle is shown due to the surface localized nature of the Ce^{3+} oxidation state in this study (a combination of normal and off angle was used to show the surface localization of the Ce^{3+} state). Peak fitting analysis was performed (AAnalyzer peak fitting software) on the Ce $3d_{5/2}$ portion of the Ce 3d photoemission spectrum in order to highlight the difference between the Ce^{3+} and Ce^{4+} states. A Ce 3d spectra of a fully oxidized Ce^{4+} surface was initially peak fitted and used as a reference. These peak fitting values were then held constant and used across each spectrum, with the difference in spectra between Ce^{4+} and Ce^{3+} attributed to the additional peak parameters obtained from subtracting the reference Ce^{4+} peak parameters. All peak values such as Gaussian, Lorentzian and binding energy positions were held constant throughout all spectra to ensure consistency. XPS spectra of both oxygen and argon plasma treated samples (held under vacuum and scanned periodically) were compared along with spectra of hydrocarbon saturated samples in order to determine the relationship between oxidation state, hydrocarbon content and wettability. Carbon elemental percentage calculations were extracted from off angle survey spectra; however, it must be noted that due to the extremely surface sensitive nature of off-angle XPS analysis used in this study, any carbon present on the surface of the sample will appear to be in a greater percentage when compared to normal emission spectra. In addition, elemental percentage calculations obtained via XPS assume a homogenous sample, which is not the case in this study (due to the surface localization of carbon), however these percentage values can be used to give a relative difference of surface carbon percentage between each sample in this study.

The reduced Ceria (III) oxidation state appears to be very surface localized as the Ce $3d_{5/2}$ narrow window scans following 96 hr. under UHV in Figure S1 shows a significant shift from normal to off angle emission spectra for the Ce $3d_{5/2}$ peak.

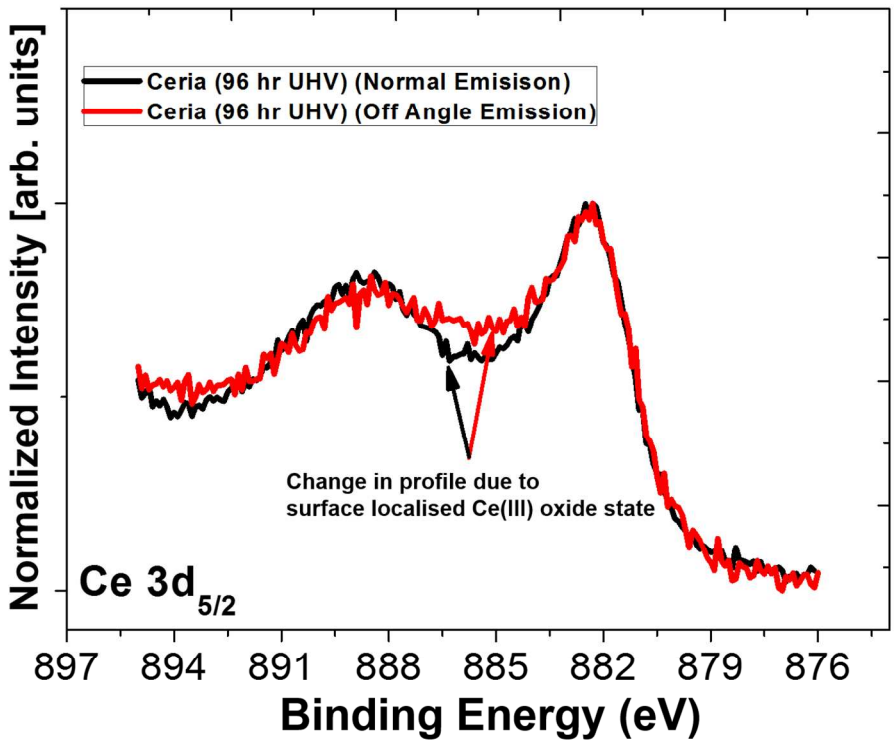

Figure S1 XPS high resolution spectra of ceria scanned after 96 hr. in UHV. The Ce 3d5/2 peak shows a change in profile from normal to off angle emission scans indicating the presence of a surface localized sub oxide state.

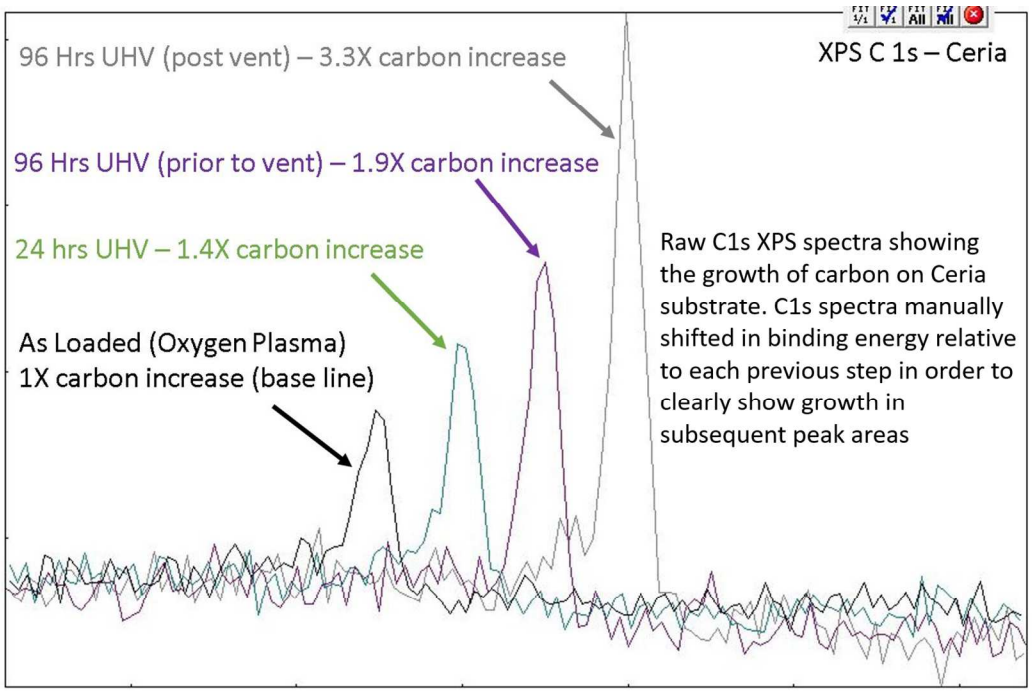

Figure S2. Carbon 1s peak as loaded, 24 hrs UHV, 96 hrs UHV and 96 hrs UHV post vent.

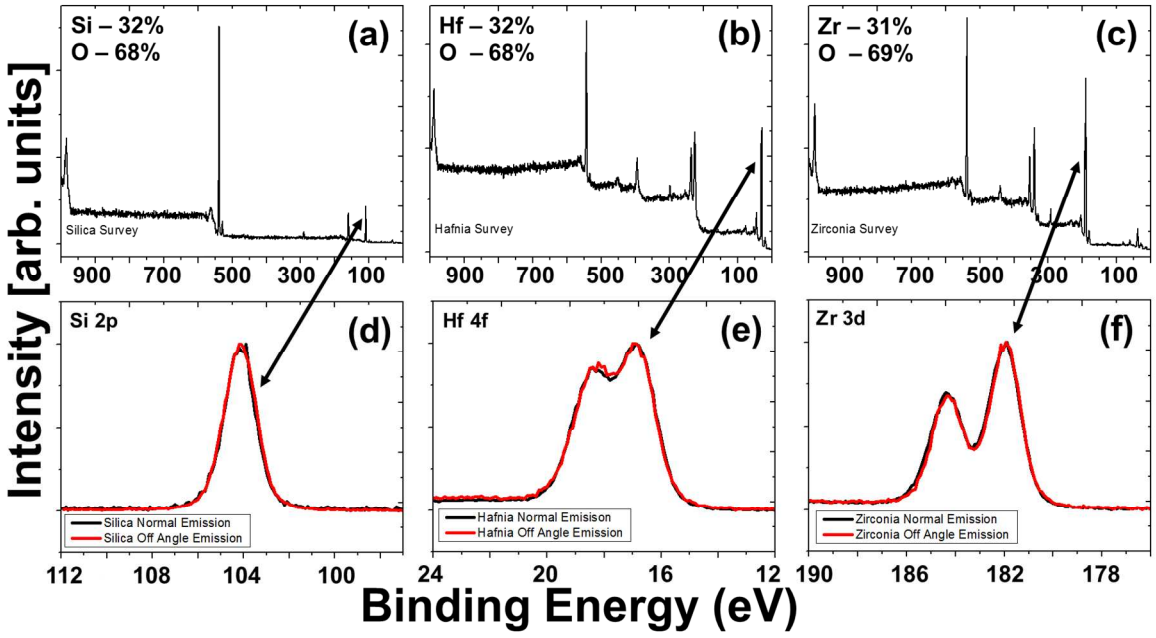

Figure S3. XPS survey spectra of (a) SiO_2, (b) HfO_2 and (c) ZrO_2 analyzed after Ar plasma treatment. Elemental composition analysis reveals the stoichiometric 4+ oxidation state for all three oxides. The high resolution spectra of (d) SiO_2 (Si 2p), (e) HfO_2 (Hf 4f) and (f) ZrO_2 (Zr 3d) indicate that the oxides are in a single stable stoichiometric state as no change in peak profile is evidenced when analyzed in both normal and off angle emission modes.

Section S2 – Samples exposed to ambient

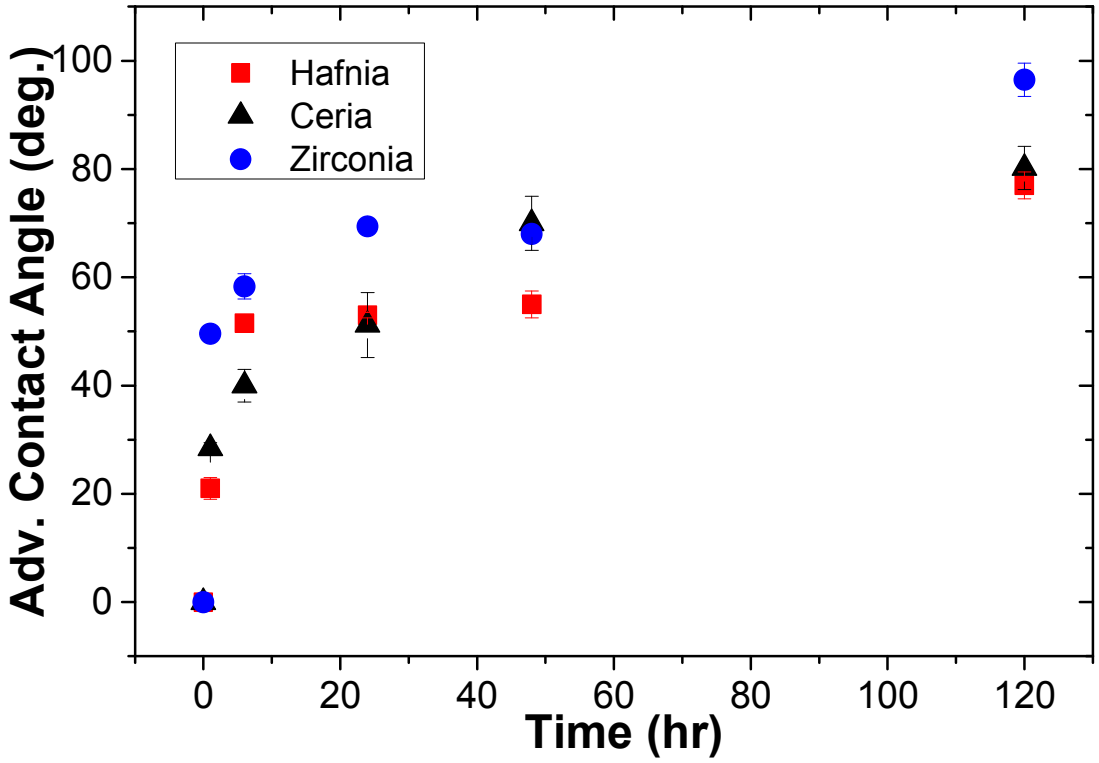

Figure S4 WCA measurements over a 120 hr. period left in ambient for Ceria, Hafnia and Zirconia. All samples are initially hydrophilic (< 10°) and become more hydrophobic (saturating at $ZrO_2 \approx 97°$, $Ce_2O_3 \approx 81°$, $HfO_2 \approx 79°$).

Section S3 – Surface coverage assuming chemical heterogeneity at the molecular scale

Surface coverage of nonane over the 96 hr. period can be calculated by considering the effects of chemical heterogeneity at the *molecular* scale: [1]

$$\Phi = \frac{(1+\cos\theta_t)^2 - (1+\cos\theta_{t=0})^2}{(1+\cos\theta_{max})^2 - (1+\cos\theta_{t=0})^2} \qquad \textit{Eq. S1}$$

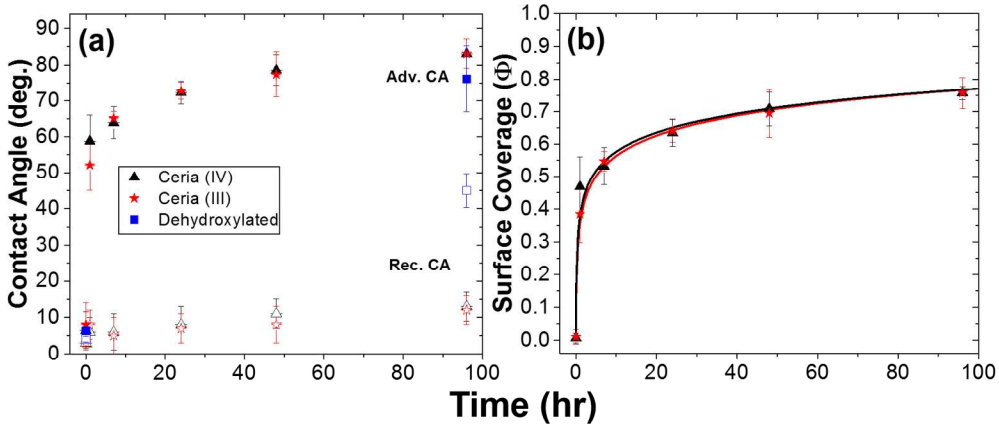

Figure S5 WCA measurements (a) over a 96 hr. period for Ceria in the (III) and (IV) oxidation state. (b) shows the evolution of surface coverage of nonane over the 96 hr. period.

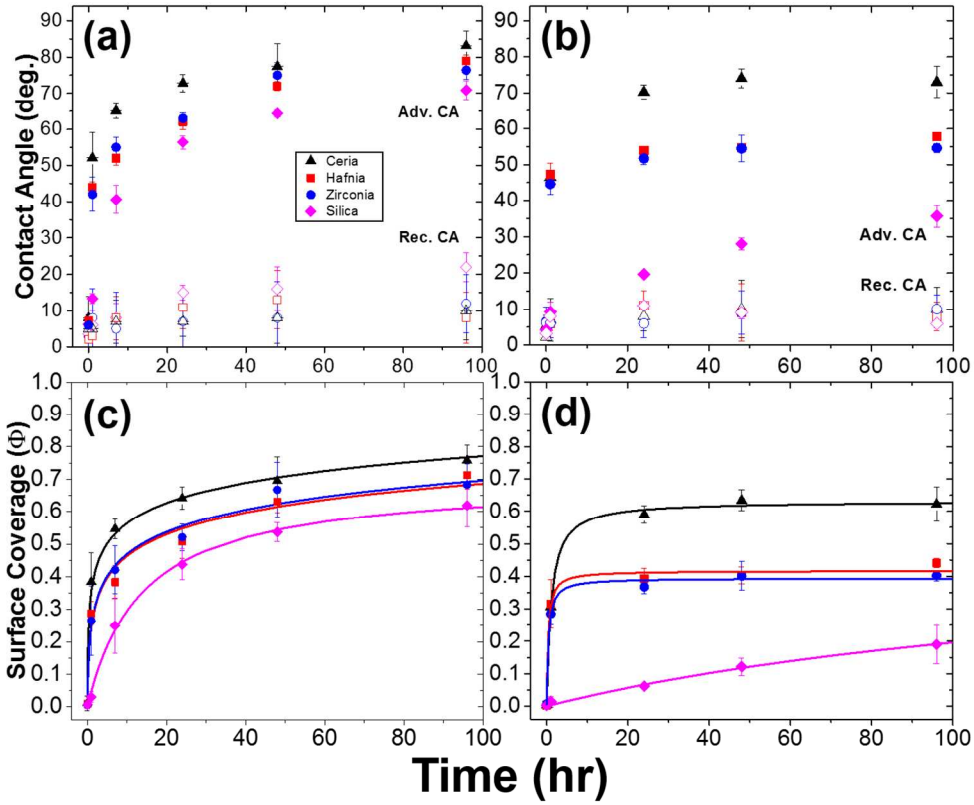

Figure S6 WCA measurements (a) and (b) over a 96 hr. period in nonane and perfluorononane respectively. (c) and (d) shows the evolution of surface coverage of nonane over the 96 hr. period.

Section S4 – Adsorption kinetics fitting

The empirical Elovich equation is typically used to fit adsorption behaviour, typically at intermediate times (this is due to the fact that the equation does not asymptote) and is used to fit data in Figure 6 (b) ($R^2 > 0.95$)

$$\Phi = \frac{2.3}{b}\ln(kb) + \frac{2.3}{b}\ln\left(t + \frac{1}{kb}\right) \qquad \textit{Eq. S2}$$

Table S1 Elovich fit parameters (Israelachvili model[1] of surface coverage)

	k	***b***	***R²***
ZrO_2/Nonane	1.3755×10^{-4}	23.318	0.989
HfO_2/Nonane	1.3682×10^{-4}	23.688	0.98
CeO_2 (IV)/Nonane	9.2413×10^{-4}	27.145	0.965
Ce_2O_3 (III)/Nonane	5.6354×10^{-4}	25.51	0.991

Table S2 Elovich fit parameters (Cassie model[2] of surface coverage)

	k	***b***	***R²***
ZrO_2/Nonane	5.89×10^{-5}	26.014	0.982
HfO_2/Nonane	5.27×10^{-5}	25.78	0.969
CeO_2 (IV)/Nonane	4.73×10^{-4}	31.46	0.975
Ce_2O_3 (III)/Nonane	2.53×10^{-4}	28.7	0.997

The empirical second order equation (SOE) can be used to fit adsorption data and is given by

$$\Phi = \Phi_{eq}\left(\frac{\Phi_{eq}kt}{1+\Phi_{eq}kt}\right) \qquad \textit{Eq. S3}$$

where *k* is the kinetic coefficient.

Table S3 SOE fit parameters (Israelachvili model of surface coverage)

	Φ_{eq}	k	R^2
SiO_2/Nonane	0.698	2.905×10^{-5}	0.998
SiO_2/Perfluorononane	0.512	3.367×10^{-6}	0.994
ZrO_2/Perfluorononane	0.395	1.778×10^{-3}	0.993
HfO_2/Perfluorononane	0.417	1.93×10^{-3}	0.987
Ce_2O_3 (III)/Perfluorononane	0.631	4.125×10^{-4}	0.997

Table S4 SOE fit parameters (Cassie model of surface coverage)

	Φ_{eq}	k	R^2
SiO_2/Nonane	0.566	2.81×10^{-5}	0.998
SiO_2/Perfluorononane	0.366	4.14×10^{-6}	0.993
ZrO_2/Perfluorononane	0.276	2.27×10^{-3}	0.994
HfO_2/Perfluorononane	0.294	2.45×10^{-3}	0.99
Ce_2O_3 (III)/Perfluorononane	0.482	4.33×10^{-4}	0.998

Apparent activation energies

Apparent activation energies for adsorption, E_a, were estimated assuming an Arrhenius form and coverage independence as

$$k = \frac{p_v}{\sqrt{2\pi MRT}} \exp\left(-\frac{E_a}{k_b T}\right), \qquad \textit{Eq. S4}$$

where k is the kinetic coefficient given in Tables S1 and S2, M is the molecular weight, R is the universal gas constant, T is absolute temperature and k_b is the Boltzmann constant.

Table S5 Apparent activation energies (Israelachvili model)

	E_a (kJ/mol)
SiO_2/Nonane	30.65
ZrO_2/Nonane	26.85
HfO_2/Nonane	26.86
CeO_2 (IV)/Nonane	22.19
Ce_2O_3 (III)/Nonane	23.4
SiO_2/Perfluorononane	36.66
ZrO_2/Perfluorononane	21.33
HfO_2/Perfluorononane	21.13
CeO_2 (IV)/Perfluorononane	24.9

Table S6 Apparent activation energies (Cassie model)

	E_a *(kJ/mol)*
SiO_2/Nonane	30.77
ZrO_2/Nonane	28.96
HfO_2/Nonane	29.23
CeO_2 (IV)/Nonane	23.87
Ce_2O_3 (III)/Nonane	25.4
SiO_2/Perfluorononane	36.15
ZrO_2/Perfluorononane	20.73
HfO_2/Perfluorononane	20.55
CeO_2 (IV)/Perfluorononane	24.79

Section S5 – Surface Energy Calculations

Since Eq. 2 (manuscript) describes surface wettability it can be used to determine γ_{sv}, the surface free energy of a solid from the advancing contact angle θ_a if the second unknown γ_{sl}, the liquid solid interfacial tension is resolved. The Fowkes theory relates γ_{sl} to the geometric means of the dispersive γ_{lv}^D and polar γ_{lv}^P solid/liquid interfacial interactions to give[3]:

$$\gamma_{sl} \approx \gamma_{lv} + \gamma_{sv} - 2\left(\sqrt{\gamma_{lv}^D.\gamma_{sv}^D} + \sqrt{\gamma_{lv}^P.\gamma_{sv}^P}\right). \quad \textit{Eq. S5}$$

Substituting Eq. S5 into Eq. 2 (manuscript) and solving gives the expression:

$$\frac{\gamma_{lv}(\cos\theta + 1)}{2} = \sqrt{\gamma_{lv}^{D}.\gamma_{sv}^{D}} + \sqrt{\gamma_{lv}^{P}.\gamma_{sv}^{P}}. \qquad \textit{Eq. S6}$$

Measuring the advancing contact angle of a surface with a liquid such as water (Table 1 of manuscript) with known dispersive and polar contributions to surface tension and solving Eq. S6 yields two unknowns, the solid's dispersive and polar contributions, γ_{sv}^{D} and γ_{sv}^{P}. Repeating this with a second liquid such as diiodomethane (Table S7) and linearizing the two equations will yield solutions to γ_{sv}^{D} and γ_{sv}^{P}. Surface energy values of H_2O – ($\gamma_{lv}^{D}/\gamma_{lv}^{P}$ = 21.8/50.8 mJ/m^2) and CH_2I_2 – ($\gamma_{lv}^{D}/\gamma_{lv}^{P}$ = 48.5/2.3 mJ/m^2)[3] were used. The calculated values for the various materials using the Fowkes theory are shown in Table 2 of manuscript.

Table S7 – Advancing (θ_a) and receding (θ_r) contact angles for various materials using diiodomethane.

Material/CH_2I_2	**0 hr (annealed)**	**300 hr (annealed)**
ZrO_2 θ_a/θ_r	40.2° ± 5.0°/ 10.5° ± 2.8°	61.9° ± 1.4°/ 34.7° ± 1.0°
Ce_2O_3 θ_a/θ_r	40.1° ± 2.0°/ 20.4° ± 1.2°	60.9° ± 1.4°/ 42.6° ± 2.2°
HfO_2 θ_a/θ_r	38.2° ± 0.2°/ 18.2° ± 0.6°	56.2° ± 0.8°/ 36.4° ± 0.6°
SiO_2 θ_a/θ_r	43.2° ± 2.0°/ 30.6° ± 1.0°	61.0° ± 1.8°/ 52.4° ± 2.0°

REFERENCES

(1) Israelachvili, J. N.; Gee, M. L. Contact Angles on Chemically Heterogeneous Surfaces. *Langmuir* **1989**, *5* (1), 288–289.

(2) Cassie, A. B. D.; Baxter, S. Wettability of Porous Surfaces. *Trans. Faraday Soc.* **1944**, *40*, 546–551.

(3) Fowkes, F. M. Attractive Forces at Interfaces. *Ind. Eng. Chem.* **1964**, *56* (12), 40–52.